sciendo

SYSTEM SAFETY: HUMAN - TECHNICAL FACILITY – ENVIRONMENT
7(1), 2025, pp. 465-481

STUDYING THE OPTICAL AND MORPHOLOGY PROPERTIES OF PMMA AND $BaTio_3/Sb_2O_3$ PMMA HYBRID NANOPARTICLES COATINGS DOPED FOR APPLICATION COATINGS SOLAR CELLS AND ELECTRONIC SCREEN

DOI: 10.2478/czoto-2025-0043
Received: 10/11/2025
Accepted: 19/12/2025

Fatima Rasheed[1], – *e-mail: mat824.fatima.rasheed@student.uobabylon.edu.iq*
Ali Salah[1] – *orcid id: 0000-0002-5038-6525, e-mail: mat.ali.salah@uobabylon.edu.iq*
Ammar Kazem[1] – *orcid id: 0000-0001-9289-2023, e-mail: mat.ammar.emad@uobabylon.edu.iq*
[1]College of Materials Engineering, Department of polymer Engineering and petrochemical industries, University of Babylon, Babylon, **Iraq**

Abstract: This article primarily aims to define the parameters related to the optical and morphological properties of solvent-cast and spun-spun coatings for coatings that offer protection against environmental conditions. It also seeks to better understand how to control the morphology and properties of coated thin films used in high-performance polymer solar cells and electronic displays to meet the protection requirements of these coatings in the aforementioned applications. This composite nano coating promotes sustainability in various ways. It increases the energy efficiency of electronic displays and solar cells, thus reducing consumption and the carbon footprint. It also enhances the durability and stability of solar cells and electronics, extending their lifespan and directly reducing electronic waste. The hybrid coating layer improves light absorption, thereby increasing the efficiency of solar and electronic cell coatings while simultaneously providing environmental protection. With increased efficiency of the hybrid materials, the efficiency of solar cells can be further improved. Hybridizing poly methyl methacrylate (PMMA) with barium titanate/antimony dioxide ($BaTiO_3/Sb_2O_3$) via solvent casting or spin coating enhances its properties, resulting in thin nanocomposites. UV-Vis spectroscopy, Fourier transform infrared (FTIR) spectroscopy, and scanning electron microscopy (SEM) were used to investigate the materials used to improve coatings for solar cells and electronic displays. The energy gap between the $BaTiO_3/Sb_2O_3$ nanoparticles decreased (from 2.4 eV for pure PMMA nanoparticles to 2 eV for PMMA nanoparticles at a concentration of 2.7 wt.%), indicating improved infrared shielding. Scanning electron microscopy revealed that the nanoparticles are homogeneously distributed, allowing for load transfer and dispersion at low concentrations (0.**9**–2.**7**%), with some agglomeration occurring at 2.7%. Infrared spectroscopy revealed physical bonds (hydrogen bonds/dipole interactions) between the nanoparticles and the PMMA material, with no chemical bonds present. The unique structure and optical properties of the nanocomposites suggest their potential for developing protective coatings with enhanced properties. Anti-reflective treatment was achieved using a simple spin-coating method based on solvent casting, resulting in a significant increase in the reflectance coefficient and the incident photon-to-

electron conversion efficiency to approximately 100 electrons in the visible spectrum. Our results demonstrate significant potential for developing high-efficiency hybrid solar cell coatings and electronic coatings, as well as hybrid nanoparticle structures, which are of considerable research interest.
Keywords: Coating, Solar Cells Coating, Electronic Screen Coating.

1. INTRODUCTION

Things, particularly metals, erode and degrade naturally due to environmental circumstances. These situations have a massive economic and environmental impact, resulting in significant financial losses and catastrophic consequences for infrastructure, industry, and ecosystems. Corrosion and environmental conditions have a significant economic impact, with estimates estimating the global cost of corrosion at trillions of dollars each year. Several strategies can be used to address these issues. One such approach is the use of polymer coatings. These coatings are designed to enhance appearance, boost mechanical durability, and protect the active ingredient from environmental factors. Regardless of the coating technique, particular polymer film properties may be assessed to evaluate coating formulations, substrate variables, and curing conditions (Obara and McGinity, 1994). Organic coatings are used in a variety of manufacturing and commercial applications, including surface protection and decorative finishes. Many popular objects are promoted only because of their surface treatment, which renders them useful. Polymers are high-molecular-weight molecules composed of several structural components connected by chemical bonds. The development of multifunctional polymer coatings has recently acquired appeal due to its usage in applications such as lowering drag in microfluidic devices, providing self-cleaning surfaces, and minimizing contamination and wear. Nano coatings have higher coefficients of thermal expansion, hardness, and durability, as well as improved abrasion and corrosion resistance (Licari, 2003). Acrylic coatings have a refractive index of 1.48 and a high light transmittance of 92%, making them suitable for optical applications. Acrylic is often molded into commercial products such as lenses, light fixtures, and attractive home furnishings. They are also used as conformal coatings on printed circuit boards and are one of the five coating types listed in MIL-I-46058. Acrylic coatings are extremely robust, scratch and abrasion resistant, and can endure temperatures ranging from -65°C to 125°C. They also have improved electrical properties, which allow for faster repair and rework. Nanostructured materials have gained appeal in recent years as a result of their improved catalytic, electrical, optical, and chemical properties. Polymer nanocomposites have aroused a lot of attention due to their unique physical properties and potential applications in a wide range of sectors. Polymer components are used in the majority of electronic devices and biological components because they are inexpensive, highly responsive, and have important electrical and physical properties. Organic-inorganic hybrid polymer nanoparticles meet a range of technological requirements. These materials are made by mixing suitable fillers with a polymer matrix to produce a single entity. The finished product's enhanced physical properties enable it to be employed as a multifunctional material in a wide range of applications (Gao et al., 2012). Organic coatings are frequently utilized for decorative and protective purposes. Organic coatings are widely accessible in a variety of colors, and their coating films can obscure the inherent colors of

coated items, giving them a more appealing look or context. Barriers are commonly employed to protect hostile equipment and structures from harsh conditions, such as maritime or industrial settings. Organic coatings change the chemical, mechanical, thermal, electrical, and optical characteristics of substrates, increasing usefulness while decreasing costs (Peesan et al., 2007; Baskaran et al., 2006). Hybrid materials have a wide range of applications, including drug delivery systems, optical and electrical devices, catalysts, photonic devices, and protective coatings (Winie et al., 2018; Carraher, 2017). The popularity of big, high-brightness computer displays has risen in recent years, as has the demand for protective coatings. The growing need for big, high-brightness displays on computer and television screens has led to the usage of nanoparticles in solar cells, electronic displays, and a range of other applications that require protective coatings (Kadhim et al., 2023). One of the most common types of nano coatings is solar cell and electronic screen coatings, which face a number of challenges that might imperil efficiency, longevity, and manufacturing quality. First, an overview of the most prevalent issues about solar cell coatings and how they affect performance; Corrosion and Environmental deterioration. Moisture may degrade metal connections and transparent conductive oxides, but galvanic corrosion happens when certain materials come into touch with moisture, resulting in an electrical potential. Harsh environments (such as coastal or industrial areas) accelerate depreciation and reduce lifetime when inadequate PECVD coatings are used. Several issues exist for solar cell coatings, which can have an impact on efficiency, durability, and manufacturing quality.

Corrosion, uneven deposition, and environmental degradation all cause concerns for solar cell coatings, lowering efficiency and lifespan. Here's an in-depth look at the most common solar cell coating difficulties and how to resolve them. Common solar cell coating issues; i. Corrosion moisture can degrade metal connections and transparent conductive oxides also where galvanic corrosion occurs when several metals react, especially in humid environments. Extreme weather conditions (such as salt spray and acid rain) accelerate the deterioration process. That means the effect reduced electrical conductivity and mechanical integrity and variable coating application. ii. Also means uneven thickness across the wafer, Particle contamination during deposition, Poor adhesion due to surface contaminants, Reduced light absorption and fluctuating cell efficiency, thus resulting in reduced energy conversion efficiency and increased maintenance costs. Coatings that crack, separate, or peel due to mismatched thermal expansion or incorrect bonding are examples of mechanical flaws. iii. Further impact the vulnerability of subgrades to environmental degradation, improved deposition technologies; PECVD systems offer greater control over plasma coefficients and substrate preparation, When we talk about protective layers, we utilize corrosion-resistant barriers and UV-stabilized polymers and quality control with real-time monitoring of the coating process to detect problems early.

So the solutions and innovation act in advanced Materials—We use multifunctional coatings that are hydrophobic, anti-reflective, and self-cleaning. Improved deposition technologies like PECVD systems offer greater control over plasma coefficients and substrate preparation. Corrosion-resistant barriers and UV-resistant polymers are two types of protective layers. Quality control; Continuous monitoring of the coating process to detect faults early. Also we can displays problems of another application like electronic screen coating: resistance to scratches and abrasion, screen coatings that are anti-reflective or oleo may erode over time, regular washing or contact with abrasive materials can erode these layers, reducing clarity and touch sensitivity, Fingerprint and Smear

Accumulation: Oleo phobic coatings repel oils but lose their effectiveness over time, resulting in more apparent smudges and a loss of screen aesthetics.
Common concerns about electronic screen coatings; i. Abrasion and Deterioration Oleo phobic coatings that remove fingerprints degrade over time, making cleaning screens more difficult. ii. Anti-reflective coatings may degrade, especially when exposed to UV light or abrasive cleaning, and scratch and abrade.
Even with protective coatings, screens are susceptible to micro-scratches from dust, keys, and rough surfaces. So we design electronic coatings provide electrical insulation and environmental protection, particularly against moisture. They protect electronics not just against moisture, chemicals, and contaminants, but also from physical damage and severe temperatures. This research discusses how functional coatings can improve the durability and performance of electronic components. Functional coatings serve numerous purposes in meeting the expanding demands of modern electronics in addition solar cells coating, including acting as protective barriers and improve optical and morphology properties for this coatings Therefore, physical solutions using multifunctional hybrid coatings with appropriate optical responses and protection, specifically tailored to the application, will be required. The aspects discussed in this chapter thus underscore the need for approaches that mitigate environmental factors in thin-film technology to achieve sustainable development and avoid negative environmental impacts. The overall understanding of the analysis reveals that thin-film applications are not immune to change, and that by introducing new ideas and engineering approaches into the manufacturing process, the sustainable use of technological resources and full protection of applications from environmental factors can be achieved, while simultaneously ensuring sustainability (Kadhim et al., 2023).

2. MATERIALS AND METHODS

2.1. Materials Used

This section will go over the materials utilized in the creation of multifunctional hybrid coatings. Table 1 shows the materials utilized, their characteristics, and their manufacturing sites. The table below lists them:

Table 1
Materials that used in this study

Product Name	Properties	Country of manufacture
Poly(methyl methacrylate) PMMA	transparency of glass with even greater impact resistance, UV stability, weathering resistance, clear, durable and unlimited coloring options.	Japan
Barium Titanate ($BaTiO_3$)	high dielectric constant, easy to use, excellent photorefractive material, strong piezoelectric properties.	China
Antimony trioxide (Sb_2O_3)	Odorless, dilute sulfuric acid, dilute nitric acid, or dilute hydrochloric acid.	China

Chloroform Solvent ($CHCl_3$)	volatile, colorless strongly smelling, and dense liquid reagent, refrigerant, and anesthetic.	China

2.2. Specimens Preparation

The coating was applied using the solution casting procedure (Sarde and Patil, 2019). PMMA nanocomposites were created by combining PMMA and ($BaTiO_3/Sb_2O_3$). The powder was vacuum-dried at 100°C for one hour. The filler and PMMA were weighed using the right ratios. Nanocomposites with 0.9, 1.8, and 2.7 wt.% hybrid filler ($BaTiO_3/Sb_2O_3$) were changed. PMMA nanocomposites were formed by thoroughly cleaning the polymer components with alcohol to remove any oil, dust, grease, or other surface impurities. The substance takes the form of particles. It was then weighed based on the stated mixing ratio. To prepare the composite, dissolve 2 g of PMMA particles in 3 ml of chloroform solution and stir for 2 hours to form a ($BaTiO_3/Sb_2O_3$) solution. This was then dissolved in 3 ml of chloroform to make a solution. The solution was then put into an ultrasonic disperser. 180W Ultrasonic Cleaner with Digital Timer and 300W Heater for Ultrasonic Cleaning at 40kHz, 6L (40 minutes before combining). The machine specifications are: Material: 304 Stainless Steel, Tank Volume: 1.8 Gallons (8 L), Ultrasonic Power: 180W, Heating Power: 300W, Ultrasonic Frequency: 40kHz, Temperature Range: 68-176°F (20-80°C), Time Range: 1-30 minutes. Basket dimensions are 11 x 5.4 x 4.5 inches (28 x 13.8 x 11.5 cm), tank measurements are 11.8 x 5.9 x 5.9 inches (30 x 15 x 15 cm), and total dimensions are 13 x 6.9 x 10.8 inches (33 x 17.5 x 27.5 cm). Net weight: 9.9 pounds (4.5 kg). Warranty period: one year. Following an hour of mixing, the solution was put into the polymer mold. Modified samples ($BaTiO_3/Sb_2O_3$) were produced using the same procedure. This process was repeated for each sample, and they were now prepared for microstructural and tribological study. Or use another process to create coating, its spin coating where is a simple thin film deposition process in its most basic form. The first phase involves preparing the polymer-solvent system, which is comparable to the solvent casting method. The substance to be deposited, which is often a polymer, is put into a suitable solvent and placed in the center of the wafer. The spin coater then quickly spins the wafer. The spinning speed, surface tension, and viscosity of the solution all have a major impact on wafer thickness. During the coating process, part of the solvent evaporates. Rapid evaporation can occasionally present issues with nanomaterials that take time to self-assemble or crystallize (Khanna, 2008). After the clear the techniques we display the samples of coating film:

Table 2
Samples and their ratio that obtained in this study

N	Sample Code	Sample Composition
1	S1	Pure PMMA
2	S2	PMMA($BaTiO_3/Sb_2$3)0.9 wt.%.
3	S3	PMMA($BaTiO_3/Sb_2$3)1.8 wt.%.
4	S4	PMMA($BaTiO_3/Sb_2$3)2.7 wt.%.

2.3. Characterization

Experimental testing is used to characterize material characteristics, which is a critical topic in engineering. Various tests have been developed throughout the years, depending

on the type of material and property to be assessed, with some becoming industry standards**.**

2.3.1. UV-Visible Absorption Spectroscopy

UV-Vis spectroscopy is the study of a sample's absorption or reflection in the ultraviolet-visible region of the electromagnetic spectrum. Absorption or reflection in the visible spectrum has a direct influence on a material's apparent color. While absorption is responsible for transitions from the ground state to the excited state, molecules in this region of the electromagnetic spectrum experience electronic transitions from the exciting to the ground state. UV-vis absorption spectroscopy was performed using an Agilent Carry 5000 near-infrared (NIR) spectrometer. The wavelength range for the scans was 300-800 nm. As shown in the structure diagram UV-visible spectroscopy (Liauw et al., 2010):

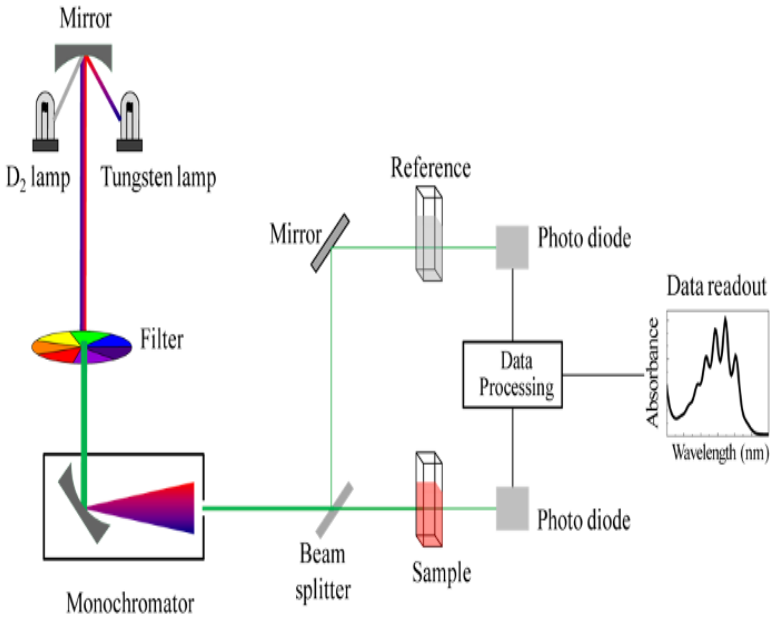

Fig. 1. Structure UV test mechanism (Liauw et al., 2010).

Optical Properties

UV-Vis and photoluminescence spectroscopy are two common spectroscopic methods for characterizing optical properties. Both methods provide information about the electrical structure of nanoparticles. A major contributor to these results is the optical properties of a material, discovered by examining its atomic structure and how the material's absorption of light affects photons as electronic signals transition within structural bands. This, in turn, reveals the energy gap, either directly or indirectly, necessitating the fitting of energy bands. Details about different types of variation constants, such as absorption coefficient, at

tenuation coefficient, and refractive index, are provided (James, 2019).

1. Absorbance (A)

In spectrophotometry, absorbance is a crucial metric for estimating the concentration of a drug in solution. It is defined as the ratio of a substance's absorbed light intensity (IA) to its received light intensity (Fawell, 2000):

$$A = log10(1/T) \quad (1)$$

$$A = log10\ (Io/I) \quad (2)$$

2. Transmittance (T)

Transmittance (T) is defined as the ratio of the intensity of the rays transmitted on the film (IT) to the intensity of the rays incident on it (Io), as stated in equation (3).

$$T = IT\ /Io \quad (3)$$

i. Absorption coefficient (α)

The absorption coefficient is defined as the percentage of energy flux reduction of the incident beam per unit distance along the incident wave's propagation direction. The absorption coefficient (α) is determined by the forbidden energy gap, material parameters, electronic transition type (n or p), and photon energy. The photon energy can be computed using the following equation (Bauckhage and Sifa, 2025):

$$E = h\upsilon \quad (4)$$

When the incident photon energy is less than the forbidden energy gap, photons will be transmitted. Equation (5) relating to transmittance is obtained.

$$T = (1 - R)2.e - \alpha t \quad (5)$$

With respect to the intensity of incident ray (Io) incident on blend film material of thickness (t), Beer Lambert law equation (6) yields the intensity of transmittance ray (I).

$$I = Ioexp(-\alpha t) \quad (6)$$

3. Optical energy gap(E_g^{opt})

i. The Electronic transitions

Essentially, there are two main types of electronic transitions:

- **Direct transition:** In semiconductors, this transition occurs when the valence band (V.B.) and the conduction band (C.B.) have the same wave vector, or $\Delta K = 0,$ and their bottoms are perfectly over each other. When $h\upsilon = Egopt,$ the absorption manifests in this condition. The conservation of momentum and energy in the law was necessary for this kind of transition. There are two kinds of direct transfers (Pankove, 2012).

Direct allowed transition: This transition presents between the top points in the (V.B.) to the bottom point in the (C.B.).

Directly forbidden transitions: This transition happens between near top points of (V.B.) and bottom points of (C.B.). The absorption coefficient for this transitions type given in equation 7 (Khanna, 2008).

$$\alpha h\upsilon = B(h\upsilon - Eg\ opt)r\ h\upsilon = Egopt, \quad (7)$$

where r is an exponential constant whose value varies according to the type of transition: r = 1/2 for permitted direct transitions and r = 3/2 for forbidden direct transitions. υ refers to the frequency of the incident photon. B is a constant that changes with the type of material.

- **Indirect transitions:** These transition types are distinguished by the bottom of (C.B.) being lower than the top of (V.B.) and the electron transiting from (V.B.) to (C.B.) in a non-perpendicular manner along the curve (E-K), with the electron's wave vector value not equal before and after the transition. ($\Delta K \neq 0$), this type of transition occurs with the particle's assistance and is known as a "Phonon" for momentum and energy conservation rules.

The limiting value of the viscosity of a material effectively at rest. This important parameter helps us understand the storage stability of suspensions, the molecular weight of polymeric materials, and the deformation behavior of materials under low stresses such as brushing.

2.3.2. Fourier Transform Infrared Spectroscopy FTIR

Fourier-transform infrared (FTIR) spectroscopy and its auxiliary optics have advanced significantly in recent years. The combination of current instruments' photometric precision, wavelength, spectrum quality, and consistency with modern chemometric methods opens up a world of new possibilities. Depending on the chemical information content, a molecule with a continuous spectrum of embedded energy can absorb light from molecules that possess that energy. The residual radiation spectrum must include an absorption band that corresponds to the frequency of the complicated vibrational and rotational motions of molecules. Infrared vibrations affecting the molecule dipole moment can be observed. Several forms of vibrations are differentiated. Vibrations are caused by the varying angles and binding strengths of the atoms in the molecule. As a result, complex molecules exhibit a diverse set of internal vibrations. In general, the frequency of the absorption band in the spectrum falls with atomic mass while increasing with bond strength constant. Vibration bands, which can be correlated with particular ligands or functional groups, make it much easier to identify unknown chemicals. The wavenumber [cm^{-}], the reciprocal of the wavelength, is commonly used to represent the position of absorption bands. This expression is proportional to the absorbed energy.

Fourier Transform Infrared (FTIR) spectroscopy of the adhesive samples was conducted using the KBr pellet technique with a Type IR Affinity-1 spectrometer (Kyoto, Japan). Each PMMA and hybrid PMMA, and Morley—was mixed with potassium bromide (KBr) in a 1:10 mass ratio. The mixtures were finely ground, pressed into pellets, and mounted onto the FTIR sample holder. The system aligned the reconstructed infrared beam with the specimen and directed it toward the detector. FTIR spectroscopy operates by analyzing the absorption, emission, or scattering of infrared radiation, enabling the identification and quantification of functional groups in bimolecular structures. It is widely employed in the characterization of biomaterials. Spectral data were recorded within the mid-infrared range of 500 to 4000 cm^{-1}. As shown in the figure 2 mechanism FTIR (Berna, 2017):

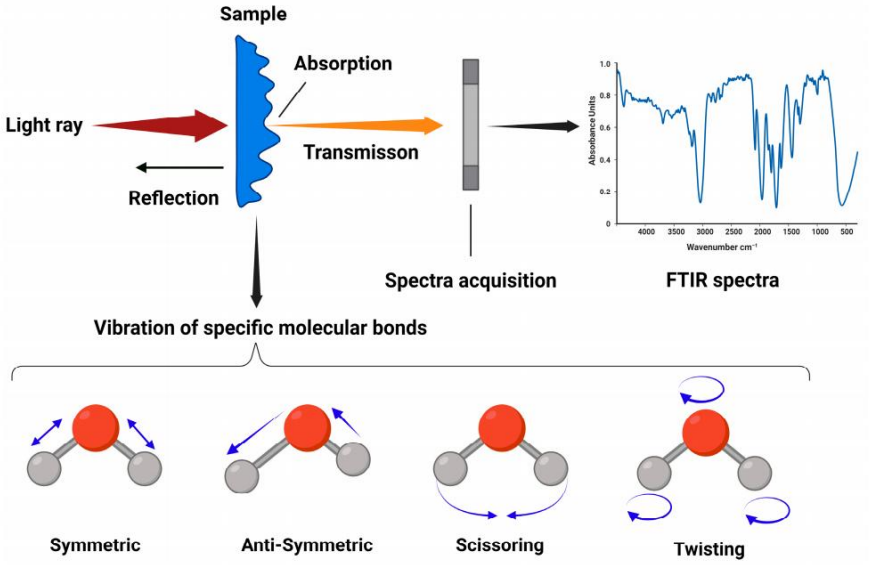

Fig. 2. Structure FTIR test mechanism (Berna, 2017).

2.3.3. Scanning Electron Microscopy(SEM)

Echoscope (TEM), which transmits electrons in the primary beam through the sample. A scanning electron microscope (SEM) scans the electron beam across the specimen's surface using a raster pattern, creating an image by mapping the observed time history to the beam position. The electron beam loses energy at each spot on the material, which is translated into other signals or photograms that reveal information about the specimen, such as its morphology and apparent composition. These include visible light, heat, pictures, secondary electrons, backscattered electrons, and diffracted backscattered electrons. The SEM image is recreated using an electron. The crystalline orientation and structure of the specimen can be predicted by analyzing the backscattered and diffracted electrons. The micro-ray phases provide insight into decomposition. Email. A scanning electron microscope consists of the source (electron gun), electron lenses, sample stage, detecting sources, display/output, and digital data requirements, as well as the computer power supply used for cooling. As shown in the figure.3 SEM mechanism (Mohammed and Abdullah, 2018):

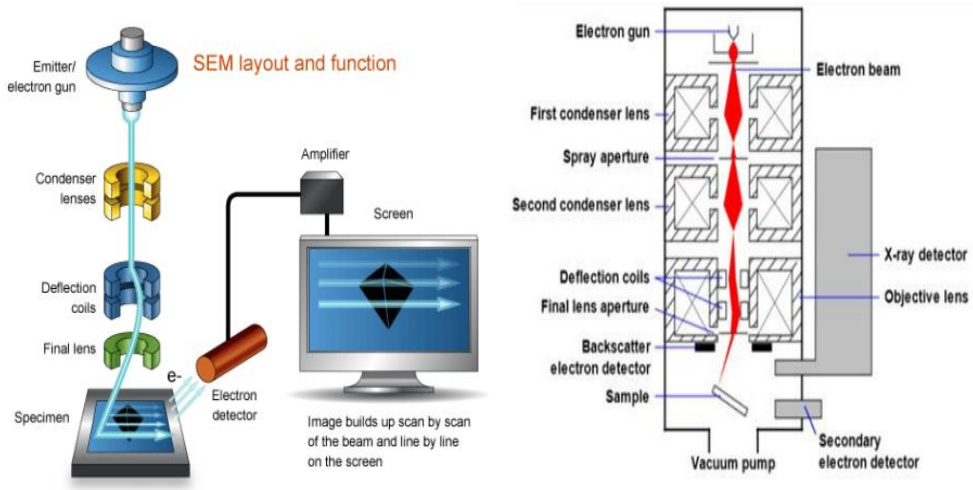

Fig. 3. Structure SEM test mechanism (Mohammed and Abdullah, 2018).

2.3.4. Wettability

Wetting occurs when a liquid and a surface make contact. A liquid with low surface tension spreads across a greater region (bonds with the surface), whereas a liquid with high surface tension (strong internal bonds) forms a droplet. The contact angle of liquid droplets (paint, water, or solvent) applied on a surface is the foundation of most wettability experiments. This angle is calculated by taking the angle produced by the surface and the droplet's surface. In general, the higher the wettability, the lower the angle. In practice, there is no angle in optimal wettability. The Young-Depret equation relates the contact angle (θ) and surface energy of the materials involved:

$$\gamma_{SV} = \gamma_{SL} + \gamma_{LV} \cos \theta \quad (8)$$

In a contact angle experiment, γ represents surface tension between two substances, whereas S, V, and L represent solid, vapor, and liquid substances, respectively. The equation can be rewritten as:

$$\gamma\, \theta\, (\cos)\, 1+ = \Delta WSLV \quad (9)$$

∆WSLV represents the adhesion energy per unit area of solids and liquids. When placed in a medium, surfaces create a V. The contact angle is often 90° or greater. It classifies a surface as non-wetting, whereas a contact angle of less than 90° shows that the surface is wet able.

The contact angle of a single liquid on a surface may be beneficial, but it does not indicate the surface's tension. Many years ago, Hansen created a simple swab test to estimate fundamental surface tension. The wet/wet-remove test is quick and simple, and it can be used on uneven surfaces where precise contact angles cannot be achieved. The fundamental test entails rubbing a solvent over a substrate and measuring whether the solvent band evaporates (shrinks or creeps) or remains in place. The critical surface tension of a substrate is determined by measuring the surface tension of the solvent with the highest surface tension. This is the tension that causes a surface to grow wet while not removing the moisture (Omer, 1975).

3. RESULTS AND DECISION

3.1. Scanning Electron Microscope Result (SEM)

SEM pictures of PMMA at 1000x magnification reveal high quantities of $BaTiO_3/Sb_2O_3$ nanoparticles. A scanning electron microscope (SEM) was used to evaluate the morphology of the PMMA and the dispersion of $BaTiO_3/Sb_2O_3$ nanoparticles within the polymer matrix (Figures 4–7). The nanoparticles are clearly disseminated throughout the PMMA matrix, with minimal agglomeration inside the polymer framework. The $BaTiO_3/Sb_2O_3$ particles (0.9 and 1.8%) are evenly distributed in the PMMA matrix, with minimal agglomeration. However, due to the higher filler density (2.7%), agglomeration occurred, resulting in a considerable number of particles distributed at the nanoscale. As the concentration of nanoparticles grew during sample fabrication, so did the matrix viscosity. Increasing the ($BaTiO_3/Sb_2O_3$) ratio led to a more brittle PMMA matrix. As witnessed during sample manufacturing, the matrix viscosity increased considerably as the concentration of nanoparticles increased. As the ($BaTiO_3/Sb_2O_3$) ratio increased, the PMMA matrix became brittle, causing a shift in surface fracture behavior from plastic to elastic. The $BaTiO_3$ surface was coated with Sb_2O_3 to guarantee complete coverage by

the PMMA matrix. The highest successful Sb_2O_3 ratio was 0.032 percent.As a result, the composite's mechanical performance improved, as did its elastic and viscoelastic recovery.

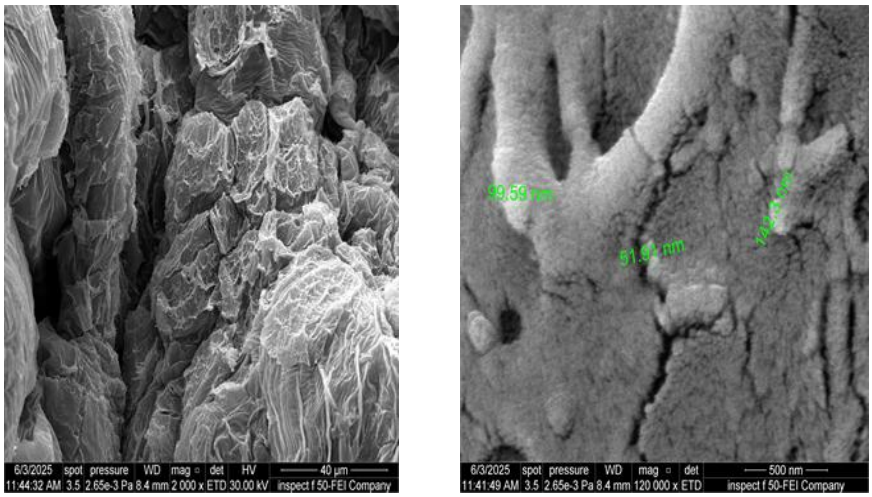

'Fig. 4. SEM of pure PMMA'

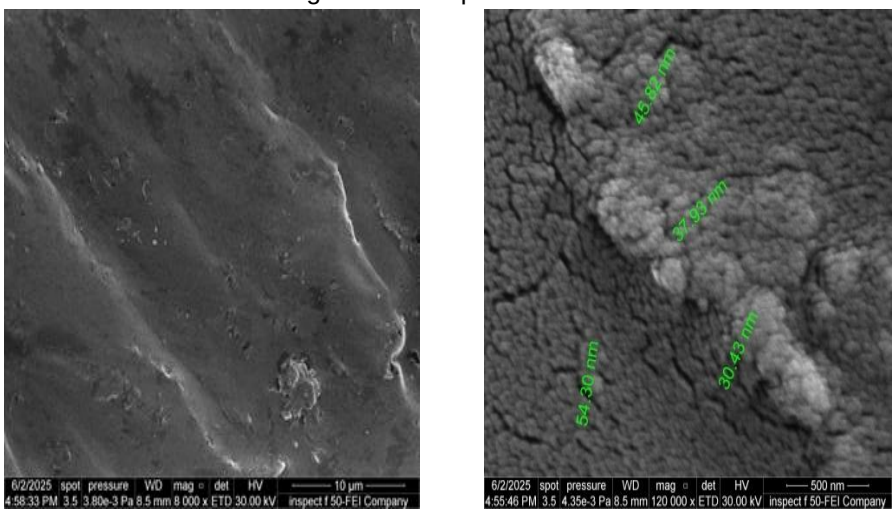

'Fig. 5. SEM of pure PMMA/($BaTiO_3$, Sb_2O_3)0.9 wt.%'

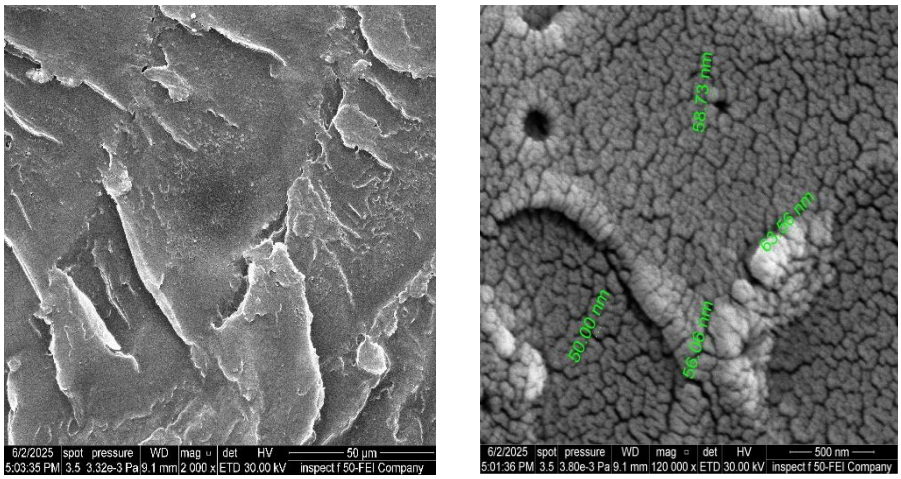

' Fig. 6. SEM of pure PMMA/($BaTiO_3$, Sb_2O_3)1.8 wt.%

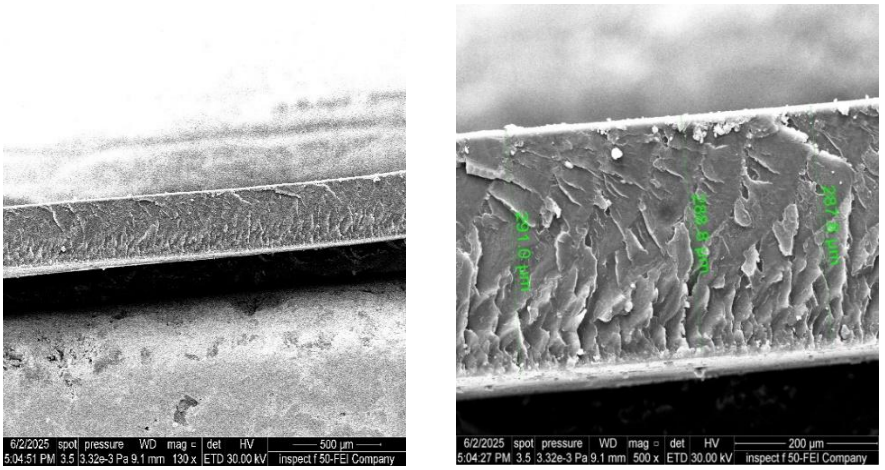

‘Fig. 7. SEM of pure PMMA/($BaTiO_3$, Sb_2O_3)2.7 wt.%

Figure 4 indicates that the surface of pure PMMA polymers is homogenous and defect-free, indicating an effective process for synthesizing these nanocomposites. Incorporating ($BaTiO_3$/Sb_2O_3) nanoparticles into a thin film alters its surface shape. Figures (5, 6, 7) show that ($BaTiO_3$/Sb_2O_3) nanoparticles are equally dispersed throughout the PMMA polymer with no agglomerations on the surface. The nanocomposite films have a smoother, more consistent shape. This outcome is consistent with the researchers findings.

3.2. Fourier transform Infrared Spectroscopy (FTIR)

Figure.8 shows the Fourier Transform Infrared (FTIR) spectra of pure PMMA and PMMA-based nanocomposites containing ($BaTiO_3$, Sb_2O_3) at three weight percentages (0.9, 1.8 and 2.7 wt.%). The spectrum of pure PMMA displays the corresponding poly methyl methacrylate absorption bands, including the strong C=O stretching vibration near 1720 cm^{-1}, the C–O–C stretching bands in the 1140–1260 cm^{-1} region, and the CH_2/CH_3 stretching bands near 2850–3000 cm^{-1}, confirming that PMMA retained its structure, and indeed serves as baseline data for observing the effects of combining nanoparticles into the polymer. The addition of ($BaTiO_3$, Sb_2O_3) to PMMA led to considerable changes in intensity and position of select carbonyl and C–H stretching bands. The loss of transmittance across the carbonyl and C-H stretch regions of the spectrum strongly suggests that intermolecular interactions between the polymer matrix and ceramic/oxide fillers occurred. Intermolecular interactions could be the result of hydrogen-bonding or dipole–dipole forces between functional groups of PMMA and the polar surfaces of $BaTiO_3$ and Sb_2O_3. Moreover, the effects of filler concentrations from 0.9 to 2.7 wt.% would indicate stronger interfacial bonding and restriction of polymer chain movement. The progressive changes of spectral features suggest that these nanoparticles are not only passively distributed but rather take part in changing the local chemical environment of PMMA. This behavior shows an increase in compatibility between the polymer and the hybrid fillers, which could lead to thermal stability, dielectric properties, and mechanical reinforcement. Thus FTIR analysis confirms the successful incorporation of ($BaTiO_3$, Sb_2O_3) composite material into the PMMA matrix and structural change from adding filler composition.

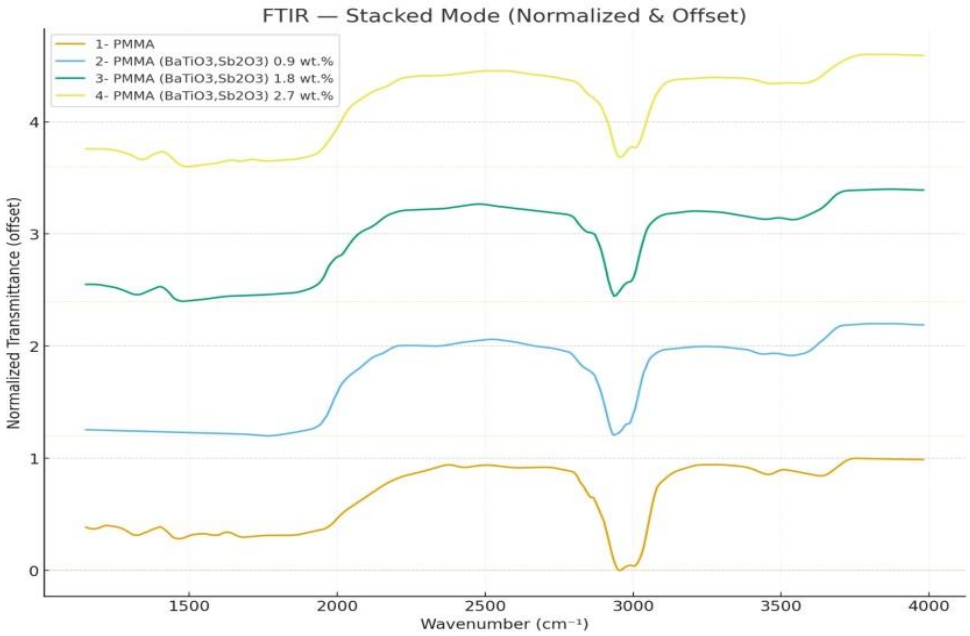

Fig. 8. FTIR of pure PMMA and PMMA/($BaTiO_3$, Sb_2O_3)0.9, 1.8 and 2.7 wt.%

3.3. Ultra -Violent Visible (U.V) Results

The thin coating of PMMA/ $BaTiO_3/Sb_2O_3$ (suggests that the transmission is low and the strength of the hole is weak with increasing awareness of ($BaTiO_3/Sb_2O_3$), this indicates that the hole is beneficial in blocking off infrared (IR) radiation, as demonstrated in Figures.9 While the low transmission suggests that there is little to no IR energy available to the film, the low electricity hole shows that the movie has a small range of energy levels that it absorbs IR radiation. This mixture's composition makes the thin movie coating appropriate for blocking IR. When the movie's material comes in contact with the thin movie layer, it may take in infrared light. Absorption occurs when the photons of infrared power are equivalent to the energy levels in the film's low-power hole. Ultimately, the movie produces a warmth that prevents the movie from flowing via the coating. The infrared radiation that is absorbed is essentially "stored" in the movie, which prevents it from migrating through the coating. The thin movie layer may not be the most effective at absorbing infrared energy, however, it does reflect some of the energy that is incoming. As the wavelength increased, the (figure.9). demonstrated that although the absorption of the PMMA/($BaTiO_3/Sb_2O_3$) samples increased in conjunction with the addition of ($BaTiO_3/Sb_2O_3$) , the absorption of the alternative samples remained constant . The movie's spectrum of transmission is demonstrated in Figures. the spectrum is proven to decrease with increased attention, this demonstrates the legitimacy of the findings. Despite now not following the strength conservation rule quite as closely, the transmission decreases as the absorption increases. This is associated with an increase in the rate of service provision and the aggregation of nanoparticles that have a higher concentration of 18. By absorption and reflection, the thin film coating that successfully prevents the passage of infrared light. The electricity that is absorbed is misdirected as heat in the movie, while the energy that is meditated is diverted away from the coated surface. Ultimately, the coating blocks infrared radiation from reaching the components beneath or surrounding it.

The movies created had a significant sized gap in the electric field, as evidenced by the computed distance between the electrodes (Figures.9). The value of the hole decreased

as materials that were halfway complete were delivered. This is because optical conductivity, which is inversely proportional to the electricity cost, is enhanced by the chemicals present in the strength gap, the distance is reduced by secondary levels that decreased their size. Table.3 shows the significance of the strength hole to PMMA and PMMA ($BaTiO_3/Sb_2O_3$).

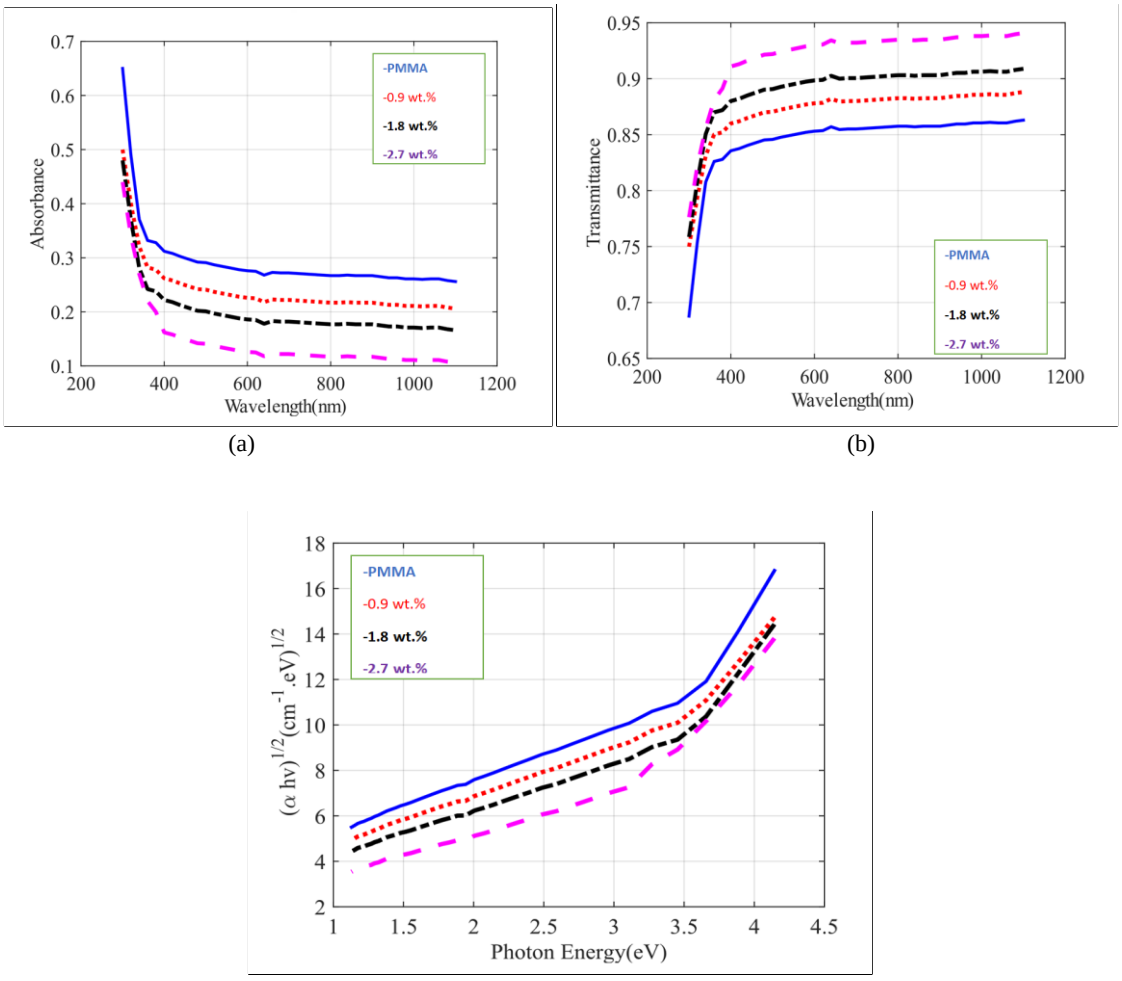

Fig. 9. a**)** Variation of absorbance with wavelength. b) Variation of transmittance with wavelength c) $(\alpha h\upsilon)^{1/2}$ Variation with photon energy for (PMMA)\ $BaTiO_3$, Sb_2O_3 nanocomposites

Table 3
Values of energy gap of samples

N	Sample Code	Energy Gap
1	S1	2.4
2	S2	2.3
3	S3	2.1
4	S4	2

3.4. Contact Angel Test

The wettability of the final coating was measured. This test was carried out using a distiller at 30°C, with the contact angle measured after 30 seconds. (Figure.10) depicts the different contact angles between undistorted PMMA and its blends. Water was swiftly moved across the surface of pure PMMA, and data were collected 10,000 times, while data from the PMMA diffuser hybrid showed partially overlapping contact at the same time. As can be seen, the contact surface contains more PMMA nanoparticles. Furthermore, the stringent nano-roughness on the hydrophobic coating's surface distinguishes hybrid from free-standing wettability. This demonstrates the formable wettability of the various composites, which increases their hydrophobicity. The table (Table.4) shown the values that obtained from the test of samples:

Table 4
Values of Contact Angle

N	Sample Code	Cav after 1S	Cav after 240S
1	S1	63.740	46.229
2	S2	96.210	90.033
3	S3	98.010	91.102
4	S4	101.032	93.071

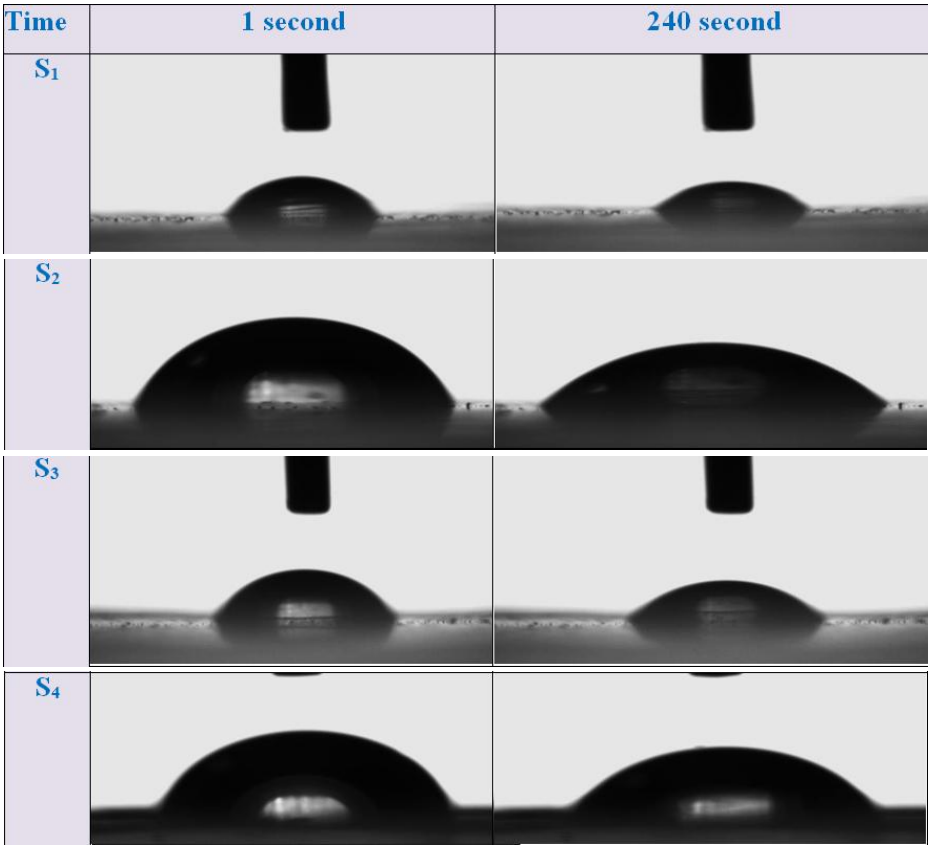

Fig. 10**.** displays the findings that were gathered from the experiment. This is indicated by the contact angle value of the PMMA, while ($BaTiO_3$, Sb_2O_3) there is increasing contact angel of compare with pure PMMA%. This can be attributed to the addition of an optimal amount of ($BaTiO_3$, Sb_2O_3) nanoparticles

4. CONCLUSIONS

This study looked regenerative functional coatings based on nano polymers represent a promising class of sustainable applications, combining the optical and chemical advantages of nanostructures with the environmental benefits of the polymers derived from them. It improves energy efficiency in electronic screens and sensors, lowering their power consumption and carbon footprint. Furthermore, it improves the durability and thermal stability of solar cells and electronics, increasing product life and directly decreasing electronic waste. Its short lifespan and low carbon footprint contribute to long-term sustainability. Lifespan is important because it balances durability with the need for frequent maintenance or replacement, reducing the overall environmental impact of the material's production and disposal into solution casting to create PMMA/($BaTiO_3$/Sb_2O_3) nanocomposite films (with weight percentages ranging from 0.9 to 2.7%). The main conclusions are that hybridization independently improves the functional abilities of PMMA. This is due to steric hindrance generated by intercalary freedom, which restricts the mobility of the polymer chain. Increasing scattered UV concentration reduces energy gaps (2.4 eV → 2 eV), indicating improved infrared blocking via absorption and multi-energy processes. Expanding the SEM pictures revealed weight loadings of 0.9-1.8% with skin agglomeration at 2.7 wt.%, leading in improved balance and characteristics. Four-transform infrared (FTIR) spectroscopy demonstrated physical interactions (hydrogen bonding/dipole) between the bands and poly methacrylate (PMMA), but no covalent bonds were found. Sb_2O_3 improves optical characteristics and infrared attenuation. The inclusion of a hybrid filler enhanced the contact angle and affinity, resulting in a shift in the hydrophobicity of the coating from 46.229° for pure PMMA to 93.071° for PMMA\($BaTiO_3$, Sb_2O_3)2.7 wt.%. This new nanoscale network has tremendous potential for medical coatings that require wireless plasticity, especially in aerospace, automotive, and electronics applications.

ACKNOWLEDGEMENTS

I would like to thank all the professors and colleagues who provided intellectual and academic support during the preparation of this research. I also extend my gratitude to the educational and other institutions that made available the necessary references and materials for this work.

REFERENCES

Baskaran, R., Selvasekarapandian, S., Kuwata, N., Kawamura, J., Hattori, T., 2006. Conductivity and thermal studies of blend polymer electrolytes based on PVAc–PMMA, Solid State Ionics, 177(26-32), 2679-2682, DOI: 10.1016/j.ssi.2006.06.039

Bauckhage, C., Sifa, R., 2025. Quantum Mechanics in a Nutshell, In: Quantum Computing from Hopfield Nets: A Textbook with Python Code Examples, Springer Nature Switzerland, Cham, 203-223, DOI: 10.1007/978-3-031-99402-9_10

Berna, F., 2017. Fourier transform infrared spectroscopy (FTIR), In: Encyclopedia of Geoarchaeology, Springer, Dordrecht, 285-286, DOI: 10.1007/978-1-4020-6235-9_110

Carraher Jr, C. E., 2017. Introduction to Polymer Chemistry, CRC Press, DOI: 10.1201/9781315369488

Fawell, J., 2000. Risk assessment case study—chloroform and related substances, Food and Chemical Toxicology, 38, S91-S95, DOI: 10.1016/S0278-6915(99)00135-8

Gao, J., Bai, H., Zhang, Q., Gao, Y., Chen, L., Fu, Q., 2012. Effect of homopolymer poly(vinyl acetate) on compatibility and mechanical properties of poly(propylene carbonate)/poly(lactic acid) blends, Express Polymer Letters, 6(11), DOI: 10.3144/expresspolymlett.2012.92

James, J., 2019. Refractive index engineering using polymer nanocomposites, Doctoral dissertation, Université de Bretagne Sud; Mahatma Gandhi University, Available at: https://theses.hal.science/tel-03086200v1/file/2019theseJemyJ.pdf

Kadhim, I. A. U., Sallal, H. A., Al-Khafaji, Z. S., 2023. A review in investigation of marine biopolymer (chitosan) for bioapplications, ES Materials & Manufacturing, 21(5), 828, DOI: 10.30919/esmm5f828

Khanna, A. S. (Ed.), 2008. High-Performance Organic Coatings, Elsevier, DOI: 10.1016/B978-0-444-51605-2.X5001-4

Liauw, M. A., Baylor, L. C., O'Rourke, P. E., 2010. UV-Visible Spectroscopy for On-Line Analysis, Process Analytical Technology: Spectroscopic Tools and Implementation Strategies for the Chemical and Pharmaceutical Industries, 81-106, DOI: 10.1002/9780470689592.ch4

Licari, J. J., 2003. Coating Materials for Electronic Applications: Polymers, Processing, Reliability, Testing, Elsevier, DOI: 10.1016/B978-0-8155-1492-3.X5000-8

Mohammed, A., Abdullah, A., 2018. Scanning electron microscopy (SEM): A review, Proceedings of the 2018 International Conference on Hydraulics and Pneumatics—HERVEX, Băile Govora, Romania, 7-9, DOI: 10.xxxx/hervex.2018

Obara, S., McGinity, J. W., 1994. Properties of free films prepared from aqueous polymers by a spraying technique, Pharmaceutical Research, 11(11), 1562-1567, DOI: 10.1023/A:1018949502392

Omer, M. A., 1975. Elementary Solid State Physics, Addison-Wesley Publishing, DOI: 10.1002/9783527619825

Pankove, J. I., 2012. Optical Processes in Semiconductors, Courier Corporation

Peesan, M., Supaphol, P., Rujiravanit, R., 2007. Effect of casting solvent on characteristics of hexanoyl chitosan/polylactide blend films, Journal of Applied Polymer Science, 105(4), 1844-1852, DOI: 10.1002/app.26918

Sarde, B., Patil, Y. D., 2019. Recent research status on polymer composite used in concrete-an overview, Materials Today: Proceedings, 18, 3780-3790, DOI: 10.1016/j.matpr.2019.07.352

Winie, T., Azmar, A., Rozana, M. D., 2018. Ionic liquid effect for efficiency improvement in poly(methyl acrylate)/poly(vinyl acetate)-based dye-sensitized solar cells, High Performance Polymers, 30(8), 937-948, DOI: 10.7317/pk.2018.42.6.1000